Direct Observation of the α-ε Transition in Shock-Compressed Iron via Nanosecond X-Ray Diffraction

D. H. Kalantar,[1] J. F. Belak,[1] G. W. Collins,[1] J. D. Colvin,[1] H. M. Davies,[2] J. H. Eggert,[1] T. C. Germann,[3] J. Hawreliak,[4] B. L. Holian,[3] K. Kadau,[3] P. S. Lomdahl,[3] H. E. Lorenzana,[1] M. A. Meyers,[5] K. Rosolankova,[4] M. S. Schneider,[5] J. Sheppard,[4] J. S. Stölken,[1] and J. S. Wark[4]

[1]*Lawrence Livermore National Laboratory, Livermore, California 94550, USA*
[2]*AWE Aldermaston, Reading, United Kingdom*
[3]*Los Alamos National Laboratory, Los Alamos, New Mexico 87545, USA*
[4]*University of Oxford, Oxford, United Kingdom*
[5]*University of California, San Diego, La Jolla, California 92093, USA*

(Received 26 April 2005; published 9 August 2005)

In situ x-ray diffraction studies of iron under shock conditions confirm unambiguously a phase change from the bcc (α) to hcp (ε) structure. Previous identification of this transition in shock-loaded iron has been *inferred* from the correlation between shock-wave–profile analyses and static high-pressure x-ray measurements. This correlation is intrinsically limited because dynamic loading can markedly affect the structural modifications of solids. The *in situ* measurements are consistent with a uniaxial collapse along the [001] direction and shuffling of alternate (110) planes of atoms, and are in good agreement with large-scale nonequilibrium molecular dynamics simulations.

DOI: 10.1103/PhysRevLett.95.075502 PACS numbers: 64.70.−p, 07.35.+k, 61.10.−i, 63.90.+t

One of the most fundamental properties of a solid is its crystallographic structure. In his Nobel-prize-winning work, Bridgman demonstrated that many crystals underwent structural transitions under the influence of static pressure [1]. Pressure-induced phase transitions were later also reported under shock compression. One of the most studied systems at high pressure is iron, due to its technological and historical importance in society, as well as its geophysical role within Earth's core [2]. A structural transformation in iron under shock loading was inferred at about 13 GPa based on wave profile measurements [3,4]. This was later identified as the α-ε phase transformation, which was observed to occur at this pressure in static experiments [5]. Despite decades of study, however, no *direct* experimental data exist confirming the crystallographic structure of this inferred transformation in shocked samples on the time scale of the shock loading process.

In this Letter, we report the first direct measurement of a structural phase transformation in shocked iron, *in situ,* and with nanosecond resolution. The data are consistent with transforming from the bcc to the hcp phase. This is the first direct observation of one of the best studied transformation processes in shock-wave physics—the α-ε transition in iron. These results are in remarkable agreement with nonequilibrium molecular dynamics (NEMD) simulations and other symmetry-proposed mechanisms, and also with complementary experiments that have been done using the technique of extreme x-ray absorption fine structure spectroscopy [6].

The very fact that the transition is thought to occur under shock conditions suggests a time scale many orders of magnitude shorter than in static experiments. Previously, an upper bound of less than 50–100 ns was inferred for the transition time from the rise time of shock waves in iron [7–9] and more recently an upper bound of less than 5 ns from the analyses of residual microstructure quenched in samples after the passage of a shock [7,10].

Several mechanisms have been proposed for the α-ε transition in iron, as described by Wang and Ingalls [11]. The first mechanism places atoms from the (110) planes into perfect hexagons by simple uniaxial compression of the bcc lattice along the [001] direction by 18.4%. An additional shuffling of alternate (110) planes by $a/3\sqrt{2}$, where a is the spacing of the initial bcc lattice, establishes the atomic ordering of a pseudo-hcp lattice where the c axis corresponds to the $[\bar{1}10]$ direction in the initial structure (Fig. 1). The second mechanism is based on shear of (112) lattice planes in the [111] direction, forcing atoms in the (110) planes into a hexagonal pattern, resulting in a compression of 13.4% and a rotation of the lattice in the (110) plane by 5°. Again, the shuffling of alternate (110) planes establishes the close-packed structure.

Recently, multimillion atom NEMD studies have explored both the mechanisms and the ultimate time scales necessary for the α-ε phase transformation in iron [12]. In these simulations, shocks of varying strength were launched along the [001] direction of defect-free single crystals of iron. At shock pressures above the transition pressure, two waves were seen to propagate within the sample. The faster of these waves corresponded to a uniaxially compressed bcc lattice, with no dislocations, plasticity, or relaxation in the directions perpendicular to the shock propagation direction [13,14]. The second wave corresponded to the transformation into the hcp phase on

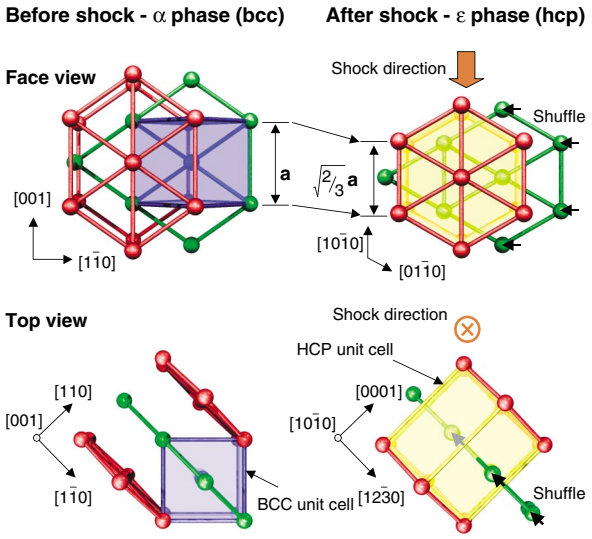

FIG. 1 (color). Schematic showing the lattice structure of the α and ε phases for iron. A pseudohexagonal structure results from 18.4% compression of the bcc lattice along [001]. Shuffling of alternate (110) planes creates the close-packed structure.

the picosecond time scale of the simulations. Above 38 GPa, a single overdriven transformation wave was observed. The resultant hcp phase was well aligned with respect to the initial bcc lattice, with the c axes corresponding to the $[\pm 110]$ directions of the original bcc crystal and consistent with the first mechanism discussed by Wang and Ingalls.

To aid interpretion of our experimental results, diffraction signals were simulated by postprocessing NEMD simulations of shocked iron [12]. For shock pressures below the transition, the reciprocal lattice is consistent with the compressed bcc lattice. Slightly above the transition pressure, the reciprocal lattice begins to show weak components due to the hcp structure. With increasing shock loading, the reciprocal lattice becomes predominantly the hcp structure. And, finally, for the highest shock pressure of 54 GPa, the atoms relax in directions perpendicular to the shock direction. The NEMD simulations have provided considerable theoretical insight into the mechanisms mediating the α-ε transition in iron.

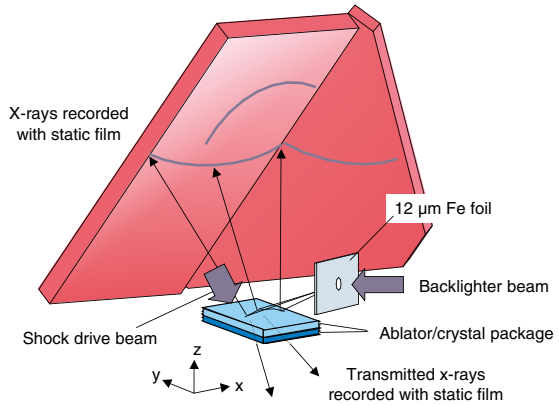

FIG. 2 (color). Schematic of the geometry used for *in situ* wide-angle diffraction measurements.

The experiments were performed using the OMEGA [15], Janus, and Vulcan [16] lasers. Samples of 200 μm thick single crystal [001] iron with a purity of 99.94% from Accumet Materials were prepared with a 16–20 μm parylene-N ablator layer and a 0.1 μm aluminum shine-through layer. These samples were shock loaded by direct laser irradiation at 2×10^{10} to 1×10^{12} W/cm^2 using 2–6 ns constant intensity laser pulses. Additional experiments were conducted using 10 μm thick single crystal samples of iron. The technique of wide-angle, *in situ* diffraction has been described previously [17–19]. Iron K-shell x rays with a wavelength of 1.85 Å were created by direct irradiation of an iron foil positioned 1.3 mm from the shocked crystal sample (Fig. 2). The x rays produced by 2–4 ns duration laser pulses diverge spherically from the source and are incident on the crystal at a range of angles. These x rays are diffracted from many different lattice planes in the crystal, resulting in line features on the film. The Bragg condition is satisfied for some planes at locations on the crystal within the region of shock loading, resulting in additional compression features.

Measurements were made at laser drive conditions that span the α-ε transition. Three sample x-ray diffraction images are shown in Fig. 3. These show lines from both the uncompressed and compressed lattice recorded as the shock propagated through the crystal. The first two images show x rays diffracted in a reflection Bragg geometry from the driven surface of the crystal, recorded with a low intensity laser drive [Fig. 3(a)] and a high intensity laser drive [Fig. 3(b)]. The image shown in Fig. 3(c) was recorded with a high intensity laser drive in transmission Bragg geometry. Individual diffraction features and lattice planes are highlighted with dashed curves, as discussed below. Details of the response of the lattice to shock loading were extracted from these images.

At a shock pressure of approximately 5.4 GPa, achieved with a laser intensity of 8.4×10^{10} W/cm^2 at 532 nm irradiation wavelength, several lattice planes show compression, shown in Fig. 3(a) with a green dashed overlay. The shifts of these diffraction lines are consistent with uniaxial compression of the lattice; namely, the atoms are displaced only along the shock direction. In this example, the compression along the [001] shock direction inferred from the shift of the (002) plane was 3.9%, and from the (112) plane was 4.1%. The error in each measurement is approximately 0.3%, based on spatial variations in the compression determined from the (002) plane.

At a higher shock pressure of approximately 26 GPa, achieved with a laser intensity of 3.1×10^{11} W/cm^2 at 351 nm irradiation wavelength, multiple compression features are evident, shown in Fig. 3(b) with both green and red dashed overlays. A nearly uniaxial compression of

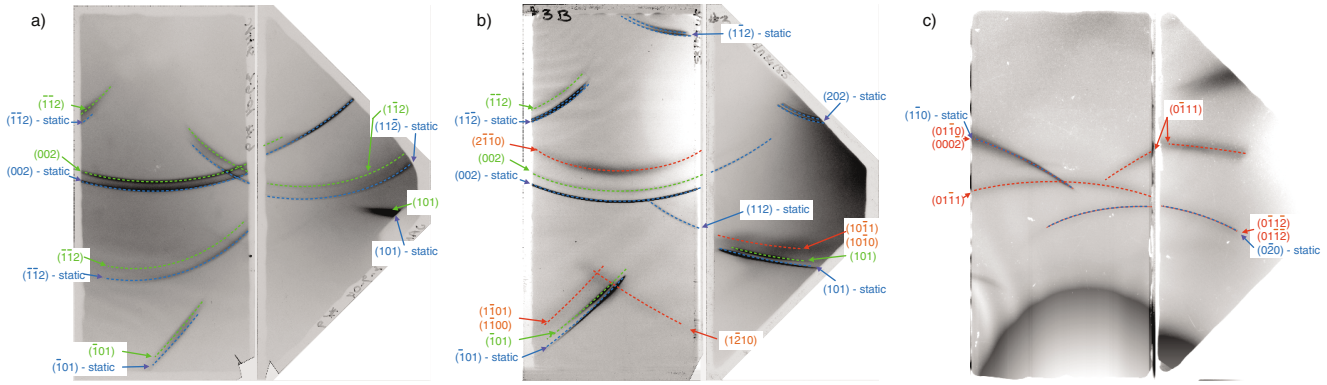

FIG. 3 (color). Sample images of the diffraction data from (a) reflection at low shock pressure, (b) reflection at high pressure, and (c) transmission geometry at high shock pressure. Lattice plane labels are based on the bcc and hcp coordinate systems defined in Fig. 1(b). Diffraction from the static bcc lattice is shown in blue, from the uniaxially compressed bcc lattice in green, and from the hcp phase in red.

approximately 6% along the (001) shock direction was observed (green overlay). Additional broader diffuse lines are evident (red overlay).

The shifted lines corresponding to uniaxial compression were analyzed in detail. The compression inferred from the (002) plane was 6.0%, whereas it was 5.5% and 5.9% from the ($\pm$1–12) and ($\pm$101) lattice planes. More detailed analysis based on fitting all the lines indicates a bulk strain of 5.5%, with a mean stress calculated from third order elasticity constants [20,21] of 11.5 GPa. This analysis showed a compression of the lattice along the [001] direction by 6%, with a slight deformation associated with shear in directions perpendicular to the shock.

The positions of the diffuse lines associated with the (002) and ($\pm$ 101) lattice planes indicate compression of the lattice along the [001] direction by 15%–18%, consistent with a transformation to the hcp structure. The additional diffuse line that does not have a corresponding static line in Fig. 3(b), and other lines that appear in the transmission diffraction images [Fig. 3(c)] are matched only by diffraction from an hcp lattice, not a compressed bcc or fcc lattice. The new feature shown in Fig. 3(b) is identified with diffraction from the (1$\bar{2}$10) lattice planes of hcp iron. The two new lines in Fig. 3(b) are consistent with diffraction from the (0$\bar{1}$11) and (01$\bar{1}$1) planes of iron. Both lines appear due to the degeneracy of the transformation along the [1 $\pm$ 10] directions.

Based on the observation of the new lines in both reflection and transmission Bragg diffraction, we conclude that the hcp phase is present, consistent with a collapse along the shock direction and the shuffling of alternate (110) planes. The time scale of this transformation is within the 2–4 ns duration of the x-ray source in this experiment. The observed symmetric shift of the diffraction from the ($\pm$101) planes suggests that there is no overall 5° rotation of the lattice, indicating that the transformation occurs by the first mechanism that is described by Wang and Ingalls [11].

The volume compression of the lattice is plotted vs shock pressure in Fig. 4. Here, this was determined as the lattice spacing parallel to the shock direction. For the uniaxial deformation up to 6%, this is from the spacing of the (002) bcc planes of the initial bcc lattice with an uncertainty of approximately 0.003. For the 15%–18% compressions, this was determined as the spacing of the [2$\bar{1}$ $\bar{1}$ 0] hcp planes with an uncertainty of approximately 0.01–0.02.

Wavelength scaling is used to relate the different experiments in Fig. 4. The drive laser wavelength was 351 nm at OMEGA, 532 nm at Janus, and 1063 nm at Vulcan. The relationship of shock pressure for a given intensity at the different wavelengths was determined from simulations using the 2D radiation-hydrodynamics code LASNEX [22]. The Janus intensities are scaled by a factor of 0.76 and the Vulcan intensities by a factor of 0.30 to relate them to the OMEGA intensities. Additional simulations indicated that

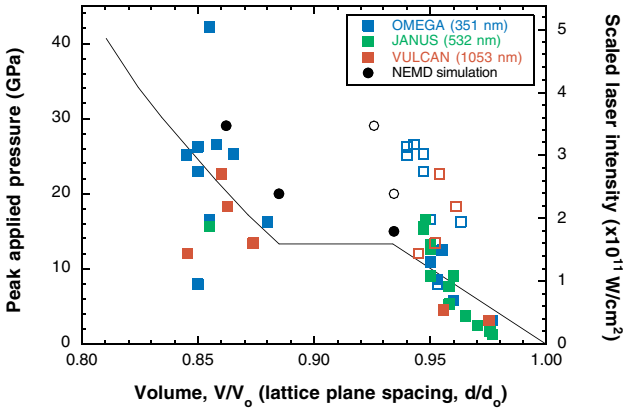

FIG. 4 (color). Volume of the compressed iron plotted vs peak drive pressure. Solid points represent the peak compression observed, and open points represent the lower compression observed for each experiment. Results from postprocessed NEMD simulations (black circles), and the room temperature shock Hugoniot are shown overlaid.

peak pressure is approximately linear with this scaled intensity at these low intensities. The compression data are plotted vs intensity in the figure.

Because of uncertainties in the preheat the crystal experiences from the low intensity laser drive, the absolute relationship of intensity to pressure scale was established based on the third order elasticity constants for iron [21]. Shock pressures were calculated for each observed compression, and an average scale factor was determined from the low-pressure experiments—those where the lattice showed only uniaxial compression. This factor was then applied to display the pressure scale on the plot. The statistical error in the mean scale factor was 10%.

The data in Fig. 4 show a discontinuity consistent with a volume collapse and phase transformation at approximately 13 GPa. Above this pressure, two compressions were observed. The lower compression (open squares) is consistent with uniaxial distortion of the initially bcc lattice and does not change with shock pressure (laser intensity). The higher compression (solid squares) is consistent with the further collapse of the lattice and transformation to hcp. Both compressions are shown on the plot to indicate their simultaneous presence in the measurements.

The results are consistent with postprocessed NEMD simulations of shocked iron, shown as black circles in Fig. 4. Above 13 GPa, the NEMD simulations show a wave separation that results in both low (7%, open circles) and high (17%, solid circles) compression features. The *in situ* diffraction results are also consistent with both the shock Hugoniot for polycrystalline iron, from Boettger and Wallace [23], shown as a solid line in Fig. 4, and the volume collapse associated with this transition in static experiments. However, the laser experiments suggest the compression is nearly uniaxial on this nanosecond time scale. Note that by using a shorter duration laser pulse to generate the x-ray probe, time resolution may be improved sufficient to observe the separation into a two-wave structure.

In conclusion, we have used the technique of nanosecond *in situ* x-ray diffraction to confirm that iron, indeed, transforms to an hcp structure under shock loading. The manner of the transformation is in remarkable agreement with previously performed NEMD simulations: the bcc lattice is compressed uniaxially by up to 6%, and there is a collapse and rearrangement consistent with the shuffle of alternate (110) planes to form the hcp phase. In both the compressed bcc phase, and the new hcp phase, there is low strain transverse to the shock propagation direction. The capability to directly observe the lattice configuration during shock compression using *in situ* diffraction offers the potential to greatly extend our knowledge of the mechanisms underlying many more shock-induced phase transformations.

This work was conducted under the auspices of the U.S. DOE by the UC LLNL and LANL under Contract No. W-7405-Eng-48. Experiments were conducted at the University of Rochester Laboratory for Laser Energetics under the NLUF grants program. Additional support was provided by the DOE under Grants No. DEFG0398DP00212 and No. DEFG0300SF2202, by the U.K. EPSRC under Grant No. GR/R25699/01, by the Advanced Simulation and Computing Materials and Physics Modeling program and LDRD-DR 20020053 at LANL, and by the LDRD program Project No. 04-ERD-071 at LLNL. The authors also acknowledge useful discussions with David Funk.

[1] P. W. Bridgman, *Collected Experimental Papers* (Harvard University Press, Cambridge, MA, 1964).
[2] F. Birch, J. Geophys. Res. **57**, 227 (1952).
[3] J. M. Walsh, Bull. Am. Phys. Soc. **29**, 28 (1954).
[4] D. Bancroft, E. L. Peterson, and S. Minshall, J. Appl. Phys. **27**, 291 (1956).
[5] J. C. Jamieson and A. W. Lawson, J. Appl. Phys. **33**, 776 (1962).
[6] B. Yaakohi *et al.*, preceding Letter, Phys. Rev. Lett. **95**, 075501 (2005).
[7] C. S. Smith, Trans. Metall. Soc. AIME **212**, 574 (1958).
[8] J. W. Forbes, Ph. D. thesis, Washington State University, 1976; Naval Surface Weapons Centre Report No. NSWC/WOL TR 77-137, 1977.
[9] G. E. Duvall and R. A. Graham, Rev. Mod. Phys. **49**, 523 (1977).
[10] T. Sano, H. Mori, E. Ohmura, and I. Miyamoto, Appl. Phys. Lett. **83**, 3498 (2003).
[11] F. M. Wang and R. Ingalls, Phys. Rev. B **57**, 5647 (1998).
[12] K. Kadau, T. C. Germann, P. S. Lomdahl, and B. L. Holian, Science **296**, 1681 (2002).
[13] B. L. Holian and P. S. Lomdahl, Science **280**, 2085 (1998).
[14] A. Loveridge-Smith *et al.*, Phys. Rev. Lett. **86**, 2349 (2001).
[15] T. R. Boehly *et al.*, Rev. Sci. Instrum. **66**, 508 (1995).
[16] C. N. Danson *et al.*, Opt. Commun. **103**, 392 (1993).
[17] Q. Johnson, A. Mitchell, and L. Evans, Nature (London) **231**, 310 (1971).
[18] E. Zaretsky, Appl. Phys. Lett. **78**, 1 (1995).
[19] D. H. Kalantar *et al.*, Rev. Sci. Instrum. **74**, 1929 (2003).
[20] *Numerical Data and Functional Relationships in Science and Technology*, Landolt-Bornstein, New Series, Crystal and Solid State Physics, Group III, Vol. 11 (Springer-Verlag, Berlin, 1979).
[21] A. D. Ritchie, Ph.D. thesis, University of California Davis, 1969; LLNL Technical Report No. UCRL-50548, 1969.
[22] G. B. Zimmerman and W. K. Kruer, Comments Plasma Phys. Control. Fusion **2**, 51 (1975).
[23] J. C. Boettger and D. C. Wallace, Phys. Rev. B **55**, 2840 (1997).